PAPER

Lacunarity exponents

IOP Publishing Journal of Physics A: Mathematical and Theoretical

J. Phys. A: Math. Theor. **52** (2019) 115101 (12pp) https://doi.org/10.1088/1751-8121/ab0349

Lacunarity exponents

Michael Wilkinson[1,2,3], Marc Pradas[1,2], Greg Huber[2,3] and Alain Pumir[2,4,5]

[1] School of Mathematics and Statistics, The Open University, Walton Hall, Milton Keynes, MK7 6AA, United Kingdom
[2] Kavli Institute for Theoretical Physics, University of California, Santa Barbara, CA 93106, United States of America
[3] Chan Zuckerberg Biohub, 499 Illinois Street, San Francisco, CA 94158, United States of America
[4] Université de Lyon, ENS de Lyon, Université Claude Bernard, CNRS, Laboratoire de Physique, 69342 Lyon, France
[5] Max-Planck Institute for Dynamics and Self-Organization, Göttingen D-37077, Germany

E-mail: m.wilkinson@open.ac.uk, marc.pradas@open.ac.uk, greg.huber@czbiohub.org and alain.pumir@ens-lyon.fr

Received 2 November 2018, revised 16 January 2019
Accepted for publication 30 January 2019
Published 14 February 2019

Abstract

Many physical processes result in very uneven, apparently random, distributions of matter, characterised by fluctuations of the local density varying over orders of magnitude. The density of matter in the sparsest regions can have a power-law distribution, with an exponent that we term the *lacunarity* exponent. We discuss a mechanism which explains the wide occurrence of these power laws, and give analytical expressions for the exponent in some simple models.

Keywords: chaos, fractals, lacunarity

(Some figures may appear in colour only in the online journal)

1. Introduction

Large fluctuations of the density of particulate matter feature in many different physical contexts. Examples include the distributions of galaxies in the universe [1], the distributions of stars within galaxies [2], the distribution of debris floating on fluids [3–5], the distribution of human populations [6] and the distribution of small inertial particles in a turbulent flow [7]. Many of these distributions are fractal [8, 9], and can be characterised by a power law, with an exponent related to one or more fractal dimensions. In particular, the density correlation function has a power-law decay, which can be related to what is known in dynamical systems theory as the correlation dimension, D_2 [10, 11].

Fractal dimensions are well adapted to characterise the densest regions of the distribution: their definition involves considering moments of the mass (or some other measure) inside a

small ball of radius ε, and taking the limit as $\varepsilon \to 0$ [8, 9]. It can be equally valuable to understand the sparse regions of the distribution. By way of examples, occupying regions of a galaxy which have a low concentration of stars reduces the risk to evolving life due to supernovae, and sparsely populated geographical regions afford protection from epidemics. However, these sparse regions have received little attention in the literature. Figure 1 illustrates an example of the prevalence of these low-density regions: it shows the distribution of density of particles position, determined from a two-dimensional, compressible flow model of transport on the surface of the ocean (the details of this simulation, and other numerical studies, are described in the section 5). There are large variations of particle density ρ, on length scales which are large compared to the correlation length ξ of the model. The numerically determined probability density function (PDF) of the particle density for this model, $P(\rho)$, shows two linear asymptotes in log-log representation, see figure 2. This indicates different power-law exponents, at high and at low densities, respectively. We denote by α the *lacunarity exponent* at low densities:

$$P(\rho) \sim \rho^{-\alpha} \text{ as } \rho \to 0. \tag{1}$$

The exponent that characterises the high-density regions is denoted as β.

Most of the potential applications described in the introductory paragraph may be described by dynamical systems which generate apparently unpredictable motion. For this reason, the models that we shall consider are all smooth, chaotic dynamical systems. The existence of a power law at high densities is consistent with the notion that chaotic systems can have fractal invariant measures [10, 11] resulting from accumulation of trajectories in converging regions of phase space. It would be natural to hypothesise that the occurrence of a power-law distribution at low densities, as shown in figure 2, might be another aspect of this phenomenon. We shall argue, however, that there is a fundamental difference between the processes responsible for creating the low and high density regions. We describe here a general approach to understand the sparse regions of the phase space of a broad class of complex dynamical systems, detailing a mechanism explaining why those sparse regions have a power-law distribution of density, and discuss examples where the lacunarity exponent α can be calculated.

'Lacunarity' as a measure of the spatial inhomogeneity of fractal sets was introduced by Mandelbrot [8], and various approaches to defining lacunarity have been explored since [12, 13]. These earlier approaches did not consider the probability distribution of density. Inhomogeneities in the clustering of fractal sets can also be characterised using the concept of multifractality (as defined by, say, Halsey *et al* [14]), but we shall argue that our lacunarity exponent is a distinct notion. In fact, while all of the models that we consider are multifractals, none of the examples of multifractal measures discussed in [14] has a lacunarity exponent. In the concluding section of our paper we return to considering the relationship between multifractality and our lacunarity exponent.

In the following, we analyse numerically and analytically the phenomena shown in figures 1 and 2 with a hierarchy of models, leading towards a good understanding of the lacunarity exponent α.

2. A minimal model

To explain the existence of the lacunarity exponent, we shall describe and analyse the simplest model for which we have observed its existence. This is the *correlated random walk*, defined by

$$x_{n+1} = x_n + f_n(x_n) \tag{2}$$

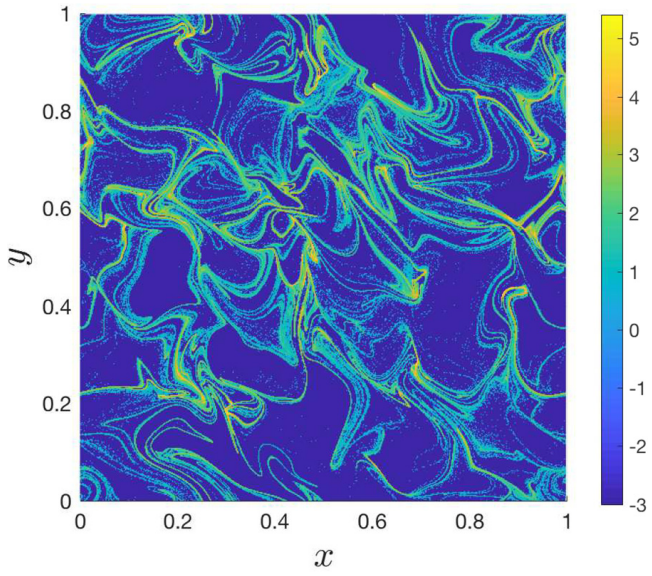

Figure 1. Distribution of particle positions in a two-dimensional random flow, mimicking the motion of debris on a sea surface. The density is inhomogeneous on length scales much larger than the correlation length ξ of the equations of motion ($\xi = 0.05$ in this illustration). The colour bar indicating density is in decimal log scale.

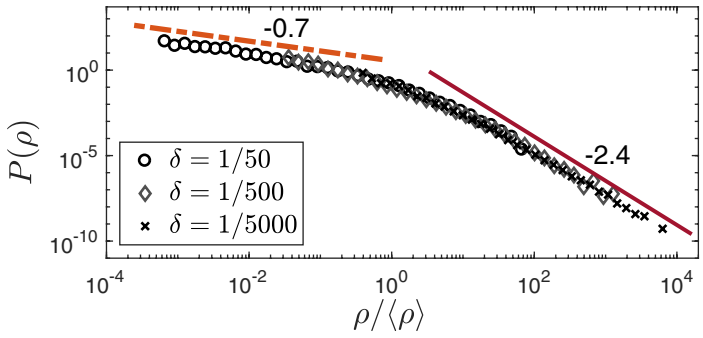

Figure 2. PDF of the particle density for the model illustrated in figure 1. There were 10^7 particles, and the densities were evaluated using square regions of size δ, much smaller than the correlation length $\xi = 0.05$, and normalised by their mean value $\langle\rho\rangle$. The two asymptotes correspond to power laws with exponents $\alpha \approx 0.7$ (low densities) and $\beta \approx 2.4$ (high densities).

where the $f_n(x)$ are random, smooth functions, drawn independently at each iteration from a Gaussian distribution. Denoting the expectation value of a number X by $\langle X\rangle$, they satisfy $\langle f_n(x)\rangle = 0$ and we choose their correlation function to have a Gaussian form

$$\langle f_n(x) f_{n'}(x')\rangle = \delta_{nn'}\epsilon^2\xi^2 \exp\left[-\frac{(x-x')^2}{2\xi^2}\right], \tag{3}$$

where ξ is the correlation length, and ϵ is a parameter for the strength of the random forcing. Because the $f_n(x)$ are differentiable functions, this model maps nearby points to nearby points, and it is arguably the simplest realisation of a dynamical system describing the motion of

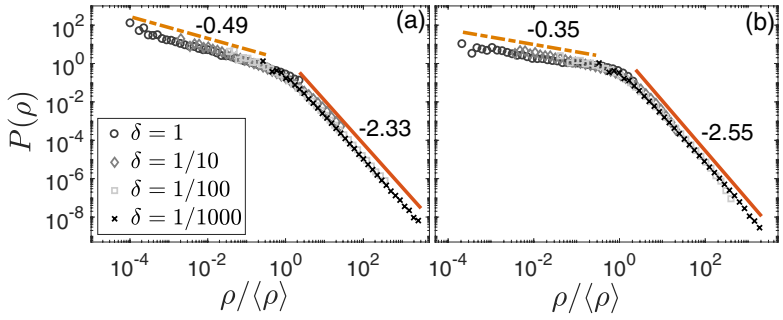

Figure 3. PDF of the density for the correlated random-walk map, equations (2) and (3), for two different values of ϵ, namely $\epsilon = 1.5\epsilon_c$ (a) and $\epsilon = 1.9\epsilon_c$ (b), ϵ_c being the critical value where the Lyapunov exponent vanishes. The PDF of the density exhibits a power law, with different exponents, in both the low- and high-density limits. The dashed and solid lines correspond to the theoretical predictions given by equations (7) and (10), respectively.

particulate objects in a complex flow field. This makes it a prototype for modelling many of the systems described in our introductory paragraph.

Because (2) is a smooth dynamical system, we can define a Lyapunov exponent in the usual manner. This one-dimensional model is chaotic (having a positive Lyapunov exponent) when ϵ exceeds a critical value $\epsilon_c \approx 1.553$ [15]. We are interested in the action of this dynamical system on a large number of points ('particles'), which are initially scattered uniformly. Because equation (2) is a non-autonomous system driven by external noise, it does not have a fixed attractor. If we average over many iterations, i.e. over the values of n, the distribution of particles averages to a uniform measure. At a fixed iteration n, however, the distribution of points is highly non-uniform. Because the map contains contracting regions, the distribution of points is expected to sample a fractal measure. The correlation dimension D_2 of this measure was obtained in [16]. The box-counting dimension dimension D_0 is equal to unity, because there are no points which do not have a pre-image.

Figure 3 shows the density distribution of final points for this model after a large number of iterations (full details of the simulation are provided in section 5). The density ρ in our numerical studies is defined empirically, using the number of trajectories $\mathcal{N}$ in a randomly chosen interval of length δ ($\rho = \mathcal{N}/\delta$). The density PDF, $P(\rho)$, was determined by dividing the range of x into bins of length δ (for the two-dimensional system illustrated in figures 1 and 2 we divided the coordinate space into squares of side δ, and defined $\rho = \mathcal{N}/\delta^2$). Figure 3 shows two power-law asymptotes, which are compared with theoretical predictions for the exponents α and β (described below). We find that both exponents approach limits as the number of iterations N increases and as the size of the interval δ decreases, provided that the total number of trajectories is large enough. The distribution of density shows clear evidence for two power-law asymptotes. We find that the exponents change continuously as the parameters of the model are varied.

3. Asymptotes of the density distribution

Now we present arguments supporting the existence of these power laws. For clarity, we start by considering the simplest case, which is a chaotic map in one dimension, such as that described by equations (2) and (3). We consider the density resulting from an initially uniform

distribution, after N iterations of the map, concentrating on the circumstances which lead to very low or very high densities. In the following, we may distinguish between the empirical density ρ, which is defined by counting particles in a small but finite interval δ, and the mathematical density $\tilde{\rho}(x)$ which is the measure obtained by taking $\delta \to 0$.

The measure contained in an interval of size δ is proportional to the total length of the pre-images of this interval. If the density in the interval is very small, the length of the pre-image intervals is correspondingly short, and the measure is proportional to the length of the interval. It follows that when we consider very small densities, the mathematical density $\tilde{\rho}$ and the finite-interval density ρ are equivalent. In the case of high-density regions, the pre-images have a length which is much greater than δ and in the limit as the number of iterations N increases, there are intervals for which the pre-image is sufficiently large that its measure does not vary linearly with δ. It follows that the distinction between ρ and $\tilde{\rho}$ is important in the high density regions where the map is contracting, so that $\tilde{\rho}$ varies very rapidly as a function of x.

If $\tilde{\rho}_N(x)$ is the density after N iterations, the density after $N+1$ iterations is

$$\tilde{\rho}_{N+1}(x) = \sum_{j=1}^{K} \left| \frac{\partial x_{N+1}}{\partial x_N} \right|_{x_j}^{-1} \tilde{\rho}_N(x_j) \tag{4}$$

where the x_j are the K pre-images of x at iteration N. We shall consider the iteration of (4) where the initial density, $\rho_0(x)$, is constant.

Because of the unpredictability of chaotic motion, we apply probabilistic methods. We formulate our argument for maps such as (2), which have Markovian properties. However, most chaotic dynamical systems are well approximated by a Markovian map if the stroboscopic interval is sufficiently large. The statistical treatment of the map from ρ_N to ρ_{N+1} simplifies in both the low- and high-density limits, leading to a power law for the probability density $P(\rho)$. We consider these in turn.

3.1. Low-density limit

First we assume that the density at x is very small. At the next iteration, where x is mapped to x', there may be other trajectories which reach x'. In general, the number K of pre-images of x' may be regarded as a random number, with a probability P_K (note that K is an odd number for continuous maps).

Consider how very small values of the density $\rho(x)$ are realised. Because the map is assumed to be chaotic, the values of factors by which the density is changed at each iteration, namely $|\partial x'/\partial x|^{-1}$, are expected to be typically less than unity, implying that the density will decrease upon iteration of the map. This tendency to produce smaller densities continues as long as there is only one pre-image. When there is a 'folding' event and there are multiple pre-images, however, the density is dominated by that arising from the largest pre-image trajectory. In the limit as $\rho \to 0$, the occurrence of a typical folding event will increase the density to a typical value. (Because low densities arise from expanding regions, we need not distinguish between ρ and $\tilde{\rho}$.) Very small values of the density are, therefore, the result of trajectories which repeatedly escape folding. Because of the Markovian nature of a map such as equations (2) and (3), the probability of surviving for m iterations without a folding event is P_1^m. In m iterations without folding, the density changes by a factor F_m which satisfies

$$\langle \ln F_m \rangle = m \left\langle \ln \left| \frac{\partial x'}{\partial x} \right|^{-1} \right\rangle_1 \tag{5}$$

where $\langle X\rangle_1$ is an average over trajectories which have only one pre-image. The distribution of the logarithm of the density, $X = \ln\rho$, therefore satisfies

$$P(X) \sim \exp\left(\frac{\ln P_1}{\langle \ln|\partial x'/\partial x|^{-1}\rangle_1} X\right) . \tag{6}$$

This implies that there is a power-law distribution of ρ of the form (1) at small values, with lacunarity exponent

$$\alpha = 1 - \frac{\ln P_1}{\langle \ln|\partial x'/\partial x|^{-1}\rangle_1} . \tag{7}$$

There is an alternative formulation of this argument which is also instructive. Consider a variable $X = \ln\rho$ instead of the density ρ. When the map is iterated, if there is only one pre-image, X is shifted by an amount $\Delta X = -\ln|\partial x_{N+1}/\partial x_N|$, which is independent of X, and which (using the Markovian assumption) may be regarded as a random variable. Furthermore, because the map has a positive Lyapunov exponent, the expectation value of ΔX is negative, so that X executes a random walk with a drift towards smaller values. However, whenever the trajectory shares a pre-image, a low density is almost certain to be dominated by that from one of the other pre-image points. This results in re-setting the value of X to a point that corresponds to a typical density. The probability for this re-set, equal to $1 - P_1$, is independent of X. These arguments indicate that, in the limit at $X \to -\infty$, the equations describing the stochastic evolution of X become independent of X. From this point the existence of a power-law distribution of ρ is a symmetry argument. The translational symmetry of the equation for iteration of X is respected by a steady-state solution for the PDF of X which is in exponential form, proportional to $\exp[(1-\alpha)X]$, for some constant α. The corresponding PDF of ρ is equation (1).

In general, incorporating the condition that there is no folding into the averaging procedure makes it extremely hard to estimate the numerator or the denominator in (7). Later we shall describe a simplified version of the model contained in (2) and (3) which does allow us to give an exact expression for α. The reasoning leading to the prediction of a power-law distribution for small values of ρ is, however, very robust. Apart from the rather mild assumption that the dynamics is chaotic and Markovian, the only additional ingredient is that there is a finite probability for a trajectory to have just one pre-image.

3.2. High-density limit

The principal result of our paper is the existence of the low-density exponent α, but it is valuable to say what we can about the high-density limit. We are able to obtain an implicit equation for the high-density exponent β for one-dimensional systems such as equation (2). The argument supporting this equation (presented below) is quite complex, and we have not found a rigorous formulation. The numerical evidence, however, provides strong support for our conclusion.

If there is only one pre-image, the value of $\tilde\rho$ is simply multiplied by $|\partial x'/\partial x|^{-1}$, which we treat as a random factor. The 'chain rule' of calculus implies that the stability factors $|\partial x_N/\partial x_0|$ evolve multiplicatively as N increases, so that they have a broad (essentially 'log-normal') distribution. This implies that for different branches (labelled by j in (4)) the stability factors can have dramatic differences in magnitude. If there are multiple pre-images, the sum components are likely to be very different in magnitude. Following arguments based upon a combination of large-deviation theory and extreme value statistics advanced in [17], in the high density

limit, the density will be dominated by the largest term in (4), so that approximating the sum by its largest term is a valid approximation when considering the limit of very high densities.

We have argued that, in the case where the density $\rho(x)$ greatly exceeds the typical value of the density, the contributions to $\tilde{\rho}(x')$ from other pre-images are almost certainly negligible, so that the transformed density is $\tilde{\rho}'(x') = \tilde{\rho}(x)/F$, where $F = |\partial x'/\partial x|$. The factor F may be treated as a random variable with probability density $\pi(F)$. After $N \gg 1$ iterations the density $\tilde{\rho}$ varies extremely rapidly as a function of the coordinate x. Let $Q_N(\rho)$ be the probability that the density at a given point is less than ρ after $N \gg 1$ iterations. At the next iteration, the cumulative probability depends upon the sensitivity factor $F(x) = |\partial x_{N+1}/\partial x_N|$: the density $\tilde{\rho}$ maps to $\tilde{\rho}' = \tilde{\rho}/F$, and intervals of length $\mathrm{d}x$ become intervals of length $\mathrm{d}x' = F\mathrm{d}x$. Let us consider the transformation of $Q_N(\rho)$ under iteration of the map. The x coordinate may be divided into intervals of length δx, which are sufficiently short that F may be approximated by a constant over each interval. Because the density varies extremely rapidly, however, each interval itself has a range of values of the density, representative of the cumulative distribution function $Q_N(\rho)$. The interval of length δx makes a contribution with weight $Q_N(x)\delta x$ to the overall cumulative distribution. After one iteration, this contribution to the cumulative weight becomes $\delta x' Q_N(F\rho)$, with $\delta x' = F\delta x$. Integrating over the distribution of F, the cumulative probability of ρ is therefore iterated as:

$$Q_{N+1}(\rho) = \int_0^\infty \mathrm{d}F\, \pi(F)\, F\, Q_N(F\rho)\ . \tag{8}$$

Seeking a steady-state solution for the PDF of the density of the form $P(\rho) = \frac{\mathrm{d}Q}{\mathrm{d}\rho} \sim \rho^{-\beta}$, we find the following implicit equation for the high-density exponent β:

$$1 = \int_0^\infty \mathrm{d}F\, \pi(F)\, F^{2-\beta}. \tag{9}$$

The existence of a power-law distribution of density in the high-density limit can be related to the fractal properties of the attractor. One characterisation of the fractal properties is achieved by considering the expectation value $\langle \mathcal{N}(\varepsilon)\rangle$ of the number of trajectories within an interval of length ε centered on a randomly chosen trajectory (thus measuring the second moment of the measure): $\langle \mathcal{N}\rangle \sim \varepsilon^{D_2}$, where D_2 is the correlation dimension [10]. It has been shown (see [16], equation (16)) that D_2 satisfies a relation closely related to (9), implying that

$$\beta = D_2 + 2\ . \tag{10}$$

4. An exactly solvable model

In the general case, the equation for the exponent α, (7), must be solved numerically. We describe one special case of the map (2) where an explicit expression for α can be obtained. Consider the map

$$x_{n+1} = x_n + F(x - \phi_n) \tag{11}$$

where $F(x) = F(x+1)$ is a periodic function, and where ϕ_n is a random number which is uniformly distributed on $[0, 1]$. Let $F(x)$ be a piecewise linear function

$$F(x) = \begin{cases} gx & 0 \leqslant x \leqslant \frac{1}{2} \\ g(1-x) & \frac{1}{2} \leqslant x \leqslant 1 \end{cases} \tag{12}$$

where $g > 0$. For this model, the forward map (11) has gradients with magnitude $1 + g$ or $|1 - g|$, both with probability $\frac{1}{2}$. The Lyapunov exponent of the model is $\lambda = \frac{1}{2}\left[\ln|g+1| + \ln|g-1|\right]$ so that the model is chaotic ($\lambda > 0$) when $g > \sqrt{2}$.

Now consider how to compute the exponents α and β which characterise the low- and high-density limits of the PDF of ρ. When $g > 1$, a point may have multiple pre-images. When $g < 3$, any point has either a single pre-image, with probability P_1, or else three pre-images, with probability $P_3 = (g-1)/2$. For this model, points which have just one pre-image all have the same expansion factor, namely $1 + g$, so that the low-density exponent, equation (7), is given explicitly by

$$\alpha = 1 + \frac{\ln(1 - P_3)}{\ln(1+g)} = 1 + \frac{\ln[(3-g)/2]}{\ln(1+g)} \,. \tag{13}$$

Equation (9) becomes the implicit equation

$$|1+g|^{(2-\beta)} + |1-g|^{(2-\beta)} = 2 \,. \tag{14}$$

Comparing this equation with (13), it is clear that no simple equation relates the exponents α and β.

5. Numerical studies

Here we give a complete specification of our numerical investigations. Figure 1 is a plot of the density of particles in a simulation of a two-dimensional flow. For this we used a simplified model

$$\boldsymbol{x}(t + \Delta t) = \boldsymbol{x}(t) + \boldsymbol{u}(\boldsymbol{x}, t)\Delta t \tag{15}$$

and the random velocity field $\boldsymbol{u}(\boldsymbol{x}, t)$ was constructed by writing

$$\boldsymbol{u} = \boldsymbol{\nabla} \wedge \boldsymbol{\psi} + \eta \boldsymbol{\nabla} \phi \tag{16}$$

where ϕ and ψ are Gaussian distributed random scalar fields which have the same isotropic, homogeneous statistics and which are independent of each other. The parameter η controls the compressibility of the velocity field (note that $\boldsymbol{\nabla} \cdot \boldsymbol{u} = 0$ when $\eta = 0$). In the simulations we used fields with $\langle \phi(x, y) \rangle = 0$ and a Gaussian correlation function:

$$\langle \phi(x,y)\phi(x',y') \rangle = \Phi \times \exp\left[-\frac{(x-x')^2 + (y-y')^2}{2\xi^2} \right] \tag{17}$$

and similarly for $\psi(x, y)$, which is statistically independent of $\phi(x, y)$. The normalization constant, Φ, was chosen so that

$$\left\langle \left(\frac{\partial^2 \phi}{\partial x \partial y} \right)^2 \right\rangle = 1 \tag{18}$$

(at every point, and similarly for $\psi(x, y)$). In figure 1 we used $\eta = 0.5$ and $\Delta t = 0.5$. The use of a large value of Δt ensures that the forward and time-reversed flows have different statistical properties, and that multiple pre-images are possible, mimicking the effect of breaking waves, for instance.

When we simulated (2), we represented the functions $f_n(x)$ by Fourier series with Gaussian distributed Fourier coefficients, with period $L \gg \xi$ (and consequently the correlation function is a periodised Gaussian). For figure 3, we used $N = 100$ iterations, and the density was

obtained by iterating 5×10^4 trajectories, in a periodic system of size $L = 5$, with $\xi = 0.5$. The points were initially uniformly scattered over $[0, L]$. Figure 3 shows a comparison between the numerically computed density PDF and the values of the exponents obtained from (7) and (10). For $\epsilon/\epsilon_c = 1.5$, these equations predict $\alpha = 0.49$ and $\beta = 2.33$ respectively, whereas for $\epsilon/\epsilon_c = 1.9$, they predict $\alpha = 0.35$ and $\beta = 2.55$, in very good agreement with the data in figure 3.

Figure 4 shows the numerically determined PDF of the piecewise-linear model, comparing the empirical exponents with the theoretical expression for α, equation (13) and with the exponent β obtained by numerical solution of (14). The numerical results provide strong evidence for power laws at both high and low densities, and even quantitative agreement with theory.

6. Generalizations

We mentioned in the introduction that power-law distributions of small densities had been observed in a variety of other contexts. Bec *et al* [18] showed that the density of inertial particles in simulations of three-dimensional turbulence has a power law at low densities, an effect also seen in a simplified model of this system [19]. Larkin *et al* [20] demonstrated that the density distribution for particles advected on the surface of a turbulent flow in a water tank shows two power-laws, at high and low densities. Kawagoe *et al* [21] discuss the distribution of weights for a model of random 'trails'. The distribution is asymptotic to a power law in the limit where the weight of a trail approaches zero, and the effect is quite distinct from the growth of voids observed close to the directed-percolation transition [22, 23]. Finally, the present authors previously reported [24] data quite closely related to figure 3, showing high- and low-density power laws for a one-dimensional model of inertial particles. These observations concern very distinct situations with quite different equations of motion, in different numbers of space dimensions, suggesting the possibility of a common mechanism giving rise to power-law behaviour.

The argument that we presented for the existence of the lacunarity exponent in the one-dimensional case hinges on two essential elements, embodied in equations (5) and (6), which can be generalised. Firstly, there must be a finite fraction of trajectories for which the volume of the pre-image of a small neighbourhood contracts exponentially backwards in time. Secondly, a mechanism must ensure that the pre-images do not continue to contract indefinitely, so that the sequence of contractions is broken. If the probability that this mechanism does not occur decreases exponentially backwards in time, then the argument supporting equation (7) implies that $P(\rho)$ has a power-law distribution as $\rho \to 0$. In the case of the one-dimensional map, the mechanism for breaking the series of pre-image contractions is the existence of multiple pre-images. Our work builds upon earlier works on the statistics of pre-images such as [25], by defining and explaining the lacunarity exponent.

These arguments apply directly to most of the previously reported examples, [18, 20, 21, 24]. The exponential reduction of density for a single trajectory with the number of iterations is a feature of all these systems: in most cases, it is a result of the exponential separation of nearby trajectories, but in [21] it is the result of trajectories randomly splitting, reducing the weight in each daughter trajectory. In all of the examples in [18–21, 24] except [20], the different trajectories can have multiple pre-images, and the probability of avoiding trajectories crossing or combining may be assumed to decrease exponentially with time. We remark that the system considered by Larkin *et al* [20] is different. This system, with the equation of motion $\dot{\boldsymbol{x}} = \boldsymbol{u}(\boldsymbol{x}, t)$, and a random velocity field $\boldsymbol{u}(\boldsymbol{x}, t)$, has a unique time-reversed motion.

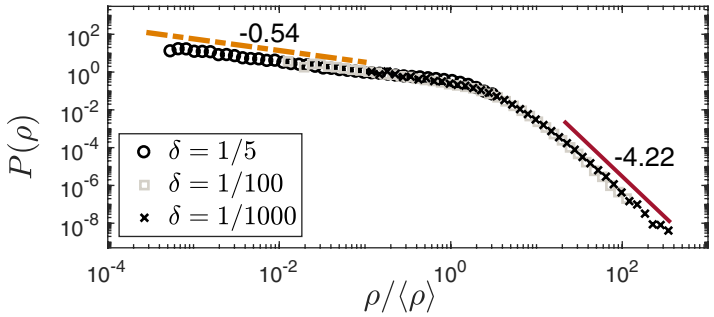

Figure 4. PDF of the density for the piecewise-linear correlated random-walk map, equations (4) and (5), with $g = \frac{7}{4}$, compared with our theory which gives $\alpha = 0.54$ (dashed line) and $\beta = 4.22$ (solid line), respectively.

Here, a different mechanism for breaking the contraction of the pre-images may play a role. The pre-images of a small disc can expand in one direction, while their area contracts. The exponential contraction of the pre-image area breaks down if the area is stretched too far, making the linear approximation inappropriate.

In the introduction we mentioned that multifractality provides another approach to understanding the inhomogeneity of fractal sets. This approach can be viewed as describing a fractal set in terms of a 'spectrum' of dimensions, by generalising the Renyi dimensions D_q, where q is the exponent of the moment of a measure [14]. The definition of these dimensions for $q < 0$ is problematic: see [26] for a discussion. It is tempting to propose that the power-law distribution of density and the exponents α and β are related to the limiting values $D_{-\infty}$ an D_{∞} of the spectrum of fractal dimensions. Our formulae for α and β in the one-dimensional case make this appear unlikely: (7) has no apparent relation to the definition of fractal dimensions, and equation (10) relates β to D_2, not D_{∞}.

If there is a relation between our lacunarity exponent α and multifractality, it would have to be a relation between α and the values of D_q for $q < 0$, because it is these dimensions which probe sparse regions via negative moments of the measure. We present below, however, a quite general argument which indicates that there can be no such relationship. The essence of the argument is that, for a very broad class of physically relevant models, including the models that we investigated in this paper, D_q is equal to the dimension of space, d, for all $q < 0$. This implies that the part of the multifractal spectrum which could describe sparsity is quite trivial.

Specifically, we consider chaotic dynamical systems for which every point has a pre-image. First, note that if there are no inaccessible regions, then box-counting dimension is $D_0 = d$. The lowest density regions determine the value of $D_{-\infty}$. At the start of section 3 we remarked that the regions with the lowest density are non-fractal, in the sense that the measure is proportional to the width of the interval. This implies that $D_{-\infty} = d$. Because D_q is a monotonic function of q, we conclude that $D_q = d$ for all $q \leqslant 0$. The 'universality' of this simple result implies that there can be no connection with the lacunarity exponent, which has a non-trivial dependence upon the parameters of the system.

7. Conclusions

In summary, we have argued that dynamical processes can produce regions of extremely sparse trajectories, characterised by a power-law distribution of density, parametrised by the lacunarity exponent, α. This property of having a power-law distribution of small densities

is complementary to the power-law distribution of high-density regions, which is associated with a fractal dimension. We have described a robust mechanism explaining the existence of this power law, and shown how the exponent can be computed for a simple system. The existence of a lacunarity exponent is consistent with existing observations in several physical contexts. It may prove to be a widely observable and quantifiable property.

Acknowledgments

MW thanks the Chan Zuckerberg Biohub for its hospitality, and all of the authors are grateful to the Kavli Institute for Theoretical Physics, where part of this research was supported by the National Science Foundation under grants PHY11-25915 and PHY17-48958. AP was supported by the IDEXLyon project (contract n°ANR-16-IDEX-0005) under University of Lyon auspices.

ORCID iDs

Michael Wilkinson https://orcid.org/0000-0002-5131-9295
Marc Pradas https://orcid.org/0000-0002-8814-2403
Greg Huber https://orcid.org/0000-0001-8565-3067
Alain Pumir https://orcid.org/0000-0001-9946-7353

References

[1] Jones B T J, Martinez V J, Saar E and Trimble V 2005 Scaling laws in the distribution of galaxies *Rev. Mod. Phys.* **76** 1211–66
[2] Elmegreen B G and Elmegreen D M 2001 Fractal structure in galactic star fields *Astrophys. J.* **121** 1507–11
[3] Yu L, Ott E and Chen Q 1991 Fractal distribution of floaters on a fluid surface and the transition to chaos for random maps *Physica* D **53** 102
[4] Sommerer J C and Ott E 1993 Particles floating on a moving fluid—a dynamically comprehensible physical fractal *Science* **259** 335–39
[5] Cózar A *et al* 2014 Plastic debris in the open ocean *Proc. Natl Acad. Sci.* **111** 10239–44
[6] Chen Y 2011 Modeling fractal structure of city-size distributions using correlation functions *PLoS One* **6** e24791
[7] Shaw R A 2003 Particle-turbulence interactions in atmospheric clouds *Ann. Rev. Fluid Mech.* **35** 183–227
[8] Mandelbrot B B 1982 *The Fractal Geometry of Nature* (San Francisco, CA: Freeman)
[9] Falconer K 1990 *Fractal Geometry: Mathematical Foundations and Applications* (New York: Wiley)
[10] Grassberger P and Procaccia I 1983 Measuring the strangeness of strange attractors *Physica* D **9** 189–208
[11] Ott E 2002 *Chaos in Dynamical Systems* (Cambridge: Cambridge University Press)
[12] Gefen Y, Meir Y, Mandelbrot B B and Aharony A 1983 Geometric implementation of hypercubic lattices with noninteger dimensionality by use of low lacunarity fractal lattices *Phys. Rev. Lett.* **50** 145–8
[13] Plotnick R E, Gardner R H, Hargrove W W, Prestegaard K and Perlmutter M 1996 Lacunarity analysis: a general technique for the analysis of spatial patterns *Phys. Rev.* E **53** 5461–8
[14] Halsey T C, Jensen M H, Kadanoff L P, Procaccia I and Shraiman B I 1986 Fractal measures and their singularities: the characterization of strange sets *Phys. Rev.* A **33** 1141–51
[15] Wilkinson M and Mehlig B 2003 The path-coalescence transition and its applications *Phys. Rev.* E **68** 040101

[16] Wilkinson M, Mehlig B, Gustavsson K and Werner E 2012 Clustering of exponentially separating trajectories *Eur. Phys. J.* B **85** 18
[17] Pradas M, Pumir A and Wilkinson M 2018 Uniformity transition for ray intensities in random media *J. Phys. A: Math. Theor.* **51** 155002
[18] Bec J, Biferale L, Cencini M, Lanotte A, Musacchio S and Toschi F 2007 Heavy particle concentration in turbulence at dissipative and inertial scales *Phys. Rev. Lett.* **98** 084502
[19] Bec J and Chétrite R 2007 Toward a phenomenological approach to the clustering of heavy particles in turbulent flows *New J. Phys.* **9** 77
[20] Larkin J, Bandi M M, Pumir A and Goldburg W I 2009 Power-law distributions of particle concentration in free-surface flows *Phys. Rev.* E **80** 066301
[21] Kawagoe K, Huber G, Pradas M, Wilkinson M, Pumir A and Ben-Naim E 2017 Aggregation-fragmentation-diffusion model for trail dynamics *Phys. Rev.* E **96** 012142
[22] Huber G, Jensen M H and Sneppen K 1995 A dimension formula for self-similar and self-affine fractals *Fractals* **3** 525
[23] Huber G, Jensen M H and Sneppen K 1995 Distributions of self-intersections and voids in $(1+1)$-dimensional directed percolation *Phys. Rev.* E **52** R2133–6
[24] Pradas M, Pumir A, Huber G and Wilkinson M 2017 Convergent chaos *J. Phys. A: Math. Theor.* **50** 275101
[25] Bec J, Gawędzki K and Horvai P 2004 Multifractal clustering in compressible flows *Phys. Rev. Lett.* **92** 224501
[26] Germinet F and Tcheremchantsev S 2006 Generalized fractal dimensions on the negative axis for compactly supported measures *Math. Nachr.* **279** 543–70